euspen's 23rd International Conference & Exhibition, Copenhagen, DK, June 2023
www.euspen.eu

End-to-end additive manufacturing for a structural aerospace component

Michiel Vlaeyen[1,2], Mirko Sinico[1,2], Ann Witvrouw[1,2], Serkan Yildiz[3], Fernando Gallego-Bordallo[4], Samuel Milton[5], Carlos Furtado[6], Wim Dewulf[1]

[1]*Department of Mechanical Engineering, KU Leuven, 3001 Leuven, Belgium*
[2]*Member of Flanders Make - Core Lab MaPS, KU Leuven, 3001 Leuven, Belgiu Belgium*
[3]*BMT Additive International N.V., 8020 Oostkamp, Belgium*
[4]*Siemens Industry Software N.V., Interleuvenlaan 68, 3001 Leuven, Belgium*
[5]*Sirris, 3590 Diepenbeek, Belgium*
[6]*Asco Industries N.V., 1930 Zaventem, Belgium*

wim.dewulf@kuleuven.be

Abstract
Additive manufacturing (AM) offers opportunities to produce three dimensional complex geometries with a greater design freedom as compared to subtractive manufacturing. New weight-saving designs are enabled, making AM an appealing production method for the aerospace industry. However metal AM for aerospace applications is currently limited to non-structural components. This paper discusses the end-to-end additive manufacturing process for a metal structural aerospace component. The object studied here is manufactured by electron beam melting (EBM) of a titanium alloy, Ti6Al4V grade 5. Software to simulate the printing process is developed in order to detect flaws in the design, which lead to deformations in the end product. The printed geometry is inspected with optical scanning and micro computed tomography (µ-CT) after each stage of the production process. The deformations predicted by the software are experimentally observed. Post-processing operations, such as hot isostatic pressure (HIP) and surface finishing, are performed to enhance the quality of the end-product. No critical internal defects are found through the µ-CT inspection. Furthermore, the deviations of all printed prototypes are within the limits of the specified tolerances, based on the comparison of the measured geometries and the nominal design performed with optical scanning.

Additive Manufacturing; Quality Inspection; Computed Tomography; Laser Scanning; Aerospace

1. Introduction

AM allows to produce complex three dimensional geometries in ready-to-use or near-net-shapes, resulting in new opportunities in terms of weight savings and freedom-of-design [1]. In this context, AM appears as an appealing production method for the aerospace industry where multiple case studies are being investigated in the last years [2-5]. However, when it comes to AM, applications are limited to non-structural components, as in the case of the A320neo fuel nozzle and the B777 T25 compressor housing temperature sensor [6], or to structural components of which fatigue is not the limiting factor while dimensioning, for instance the A320 nacelle hinge bracket or the A350 XWB bracket, due to the challenges associated with fatigue applications and the inherent limitations of current powder printing technologies. However, surface treatments can be applied to improve the quality and obtain a good fatigue strength. This paper examines the applicability of AM for a fatigue loaded structural component. This research is performed in the framework of the ALMA project [7], where an aerospace actuator lever designed by ASCO is prototyped using EBM, taking into consideration the end-to-end manufacturing process. In the conception phase, new design methods like topology optimization are associated with AM overcoming the limitations of subtractive manufacturing. Simulation tools can be used to anticipate deformations after the printing process due to thermal stresses. Since porosities and surface irregularities are common in EBM processes, post-processing steps such as HIP, and surface finishing technologies such as blasting or electropolishing, are applied to increase densification, to eliminate defects and to meet specified roughness tolerances [8]. In this context, non-destructive testing is performed not only to monitor dimensional deviations, but also to detect if porosity and cracks, that originated during the AM process, are reduced to acceptable levels during post-processing. However, the inherent difficulty of achieving high resolution µ-CT inspection for big and bulky parts, and the lack of reliability in serial production to detect defects that are to be avoided in safety critical applications, appears as a critical reason for the slow adoption of AM for fatigue susceptible parts.

2. Electron beam melting

The ALMA project studies prototypes produced via EBM and Laser Powder Bed Fusion (LPBF). These methods use a layer-by-layer approach to make up the end-product. In this paper only the prototypes produced by EBM are discussed. The material of the components is a titanium alloy, Ti6Al4V grade 5. Ti6Al4V is chosen as fusion material due its commercial wide availability and potential in the Aerospace industry as a lightweight material with a high strength. Furthermore, Ti6Al4V is a well-known and certified material by aerospace standards.

3. Non-destructive testing

Two types of non-destructive testing are used to analyze the different steps in the production process. Optical measurements are performed to compare the form of the produced object with the intended design and µ-CT is used to detect internal defects, i.e., porosity and cracks.

3.1. Optical scanning

The optical measurements are performed with a laser line scanner (LLS) mounted on a Coord3 MC16 coordinate measuring machine, illustrated in Figure 1. This system generates a point cloud to perform dimensional quality inspections. The point cloud is generated by projecting a laser beam on the object and the reflection is captured on the CCD sensor. The point of reflection, i.e. the intersection of the laser beam and the object, is calculated by triangulation [9]. LLSs are commonly used in reverse engineering applications and quality inspections due to their high density measured points and relative high accuracy. The Nikon Metrology LC60Dx LLS has a maximum permissible probing error of 9 µm, according to its specifications. The LLS measures the surface of the AM produced aerospace component in order to monitor dimensional deviation after each stage of the production process.

Figure 1. CMM and LLS setup.

3.2. Micro computed tomography

Aerospace specifications, like the Airbus *AIPS01-04-020*, requires the µ-CT inspection of all the parts produced via AM with strict acceptance criteria. More specifically, to reach the *Quality Level 1 – Acceptance Level A* (QL1-A), all pores ⌀ > 200 µm must be correctly identified by µ-CT (i.e., 100 % probability of detection). This goal is unrealistic for thick and dense metal components, as the current state-of-the-art high energy CT equipment presents limitations coming mainly from the blurring caused by the defocusing of the focal spot inside the X-ray gun at high energies [10,11], and secondly from the high amount of artefacts generated [12].

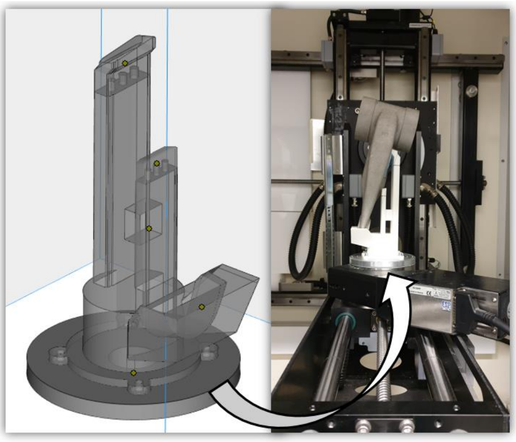

Figure 2. The ALMA prototype mounted on the Nikon XTH 450 manipulator; a special 3D printed plastic holder was designed to keep the object at a favorable scanning orientation.

Therefore, for the scope of this investigation, all ALMA prototypes were subjected to high energy µ-CT inspection while being aware that the QL1-A requirements might not be met. In details, all components were scanned in two sections, and later on merged after reconstruction, employing a Nikon XTH 450 system with scanning parameters: 420 kV, 100 µA, 10 mm Cu filter, 3142 projections with 2829 ms of exposure time for projection. The achieved voxel size was 88.7 µm, and the theoretical focal spot of the system was 80 µm. Although the resolution seems high enough to meet the desired inspection quality level for the ALMA prototypes, it must be stated that a considerable amount of beam hardening, streak-noise artefacts, and general noise coming mainly from scattering were present on the reconstructed datasets. These artefacts hamper the correct identification of pores nearby the resolution limit, pushing the probability of detection curve further to higher defect sizes. This effect is well described in the work of Sinico et al. [11], also produced in the framework of the ALMA project. Considering the DoE reported in that publication, we can estimate that, for the employed CT scanning parameters, the 100 % probability of detection is reached only for ⌀ ~ > 300 µm. Defect detection after reconstruction was performed using the VGSTUDIO MAX 3.4 software, via the VGEasyPore algorithm in subvoxel accuracy mode and with a defect refinement distance of ± 3 voxels.

4. Part production

The production process is split up in three phases: the design, the manufacturing process and the post-processing. The manufacturing process consists of the printing of the ALMA prototypes and the removal of the supports. The post-processing phase includes HIP at 920 °C / 120 min / 1000 bar, machining of assembly surfaces, i.e. “nose” and back lugs, and dry blasting of inactive surfaces, i.e. the “organic” body design, using coarse corundum. In this paper, the quality inspection focusses on the prototypes after support removal, after HIP, and after machining and dry blasting. The process flow is depicted in Figure 3. After the manufacturing phase and each post-processing step the aerospace component is inspected with the presented non-destructive testing methods.

4.1. Design

The design principles are different for additive manufacturing when compared to conventional manufacturing. Several researchers, machine builders along with the industrial users have developed a defined set of principles for DfAM (Design for Additive Manufacturing) [13-15]. A workflow based on scoring was created following different multidisciplinary criteria such as topological optimization, design for printing, design for post machining, design for surface treatments, design for inspection and design for cost. Based on these scores a final design was selected to be printed with EBM technology. Post-processing is required to remove the supports and obtain features with tight tolerance requirements. Furthermore, form deviations are to be expected due to the production method. Due to thermal stresses and heat buildup during the production, the produced object might differ from the intended design. Siemens has adapted its Simcenter 3D LPBF models and boundary conditions to compute the process-induced distortion after printing with EBM. With this purpose, the EBM pre-heating temperature has been introduced in the simulation workflow. This higher temperature range that is kept during the EBM process prevents the part from elevated residual stresses. To consider this, a stress relief simulation step has been added accordingly. Additionally, the existing calibration process for LPBF has been applied by printing the appropriate calibration specimens at BMT with the same process parameters as for the aerospace component [16]. Stiffness-dependent shrinkage parameters were derived from measurements on these specimens and used to compute process-induced distortion. Distortion results were assessed with optical data and have been compared with the EBM simulation. Obtained results show a comparable shrinkage trend to what is observed in all the printed components in as built state, as shown in Figure 4. A compensated geometry can be created with Simcenter 3D LPBF tool to avoid these deformations during the printing process.

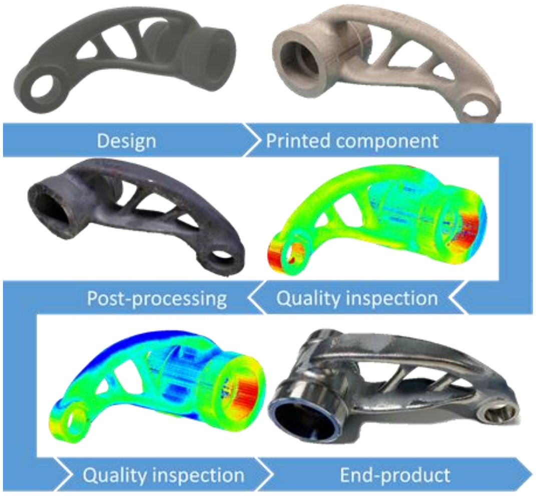

Figure 3. The prototype production.

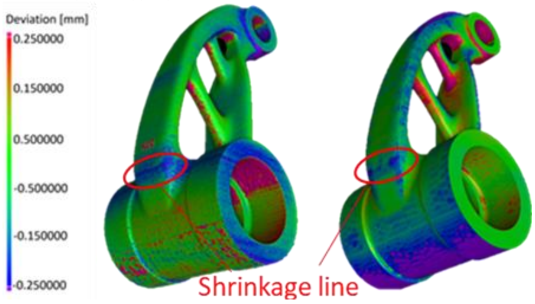

Figure 4. Experimental (left) and numerical distortion values (right).

4.2. Manufacturing process

The designed parts are produced in Ti6Al4V by EBM. After the AM process the support structures are removed. In total eight prototypes were fabricated in two build jobs, where six labeled parts were kept for further examination and two parts were scrapped. The prototypes of the first batch are labeled K01, K02 and K03, and of the second batch L01, L02 and L03. The elevated printing temperature of the EBM process allows for multiple parts to be printed at the same time with minimal use of support structures, as illustrated in Figure 5.

To be able to find the optimized process parameter sets for these parts a broad sensitivity study was performed, consisting of 105 parameter sets. The evaluation criteria included surface quality, relative density and productivity. With the optimized process parameters, the build jobs were successful first time right, without having to repeat the jobs for compensation. The printed aerospace components are measured with the LLS and the dimensional deviation from the intended design is determined. The comparison of the six prototypes, selected for the next production stages, is depicted in Figure 6. The comparison shows deviations from the design: the shrinkage line, i.e. blue zone on the left of the label, and the extension of the component, i.e. the red zone at the "nose" of the component. Both distortions were predicted with the simulation tool. Some residuals of the supports, that need to be removed during the post-processing, are still visible. Furthermore, the comparison shows that the placement of the prototypes in the printer has an influence. While all the components are produced with identic printer settings, the prototypes at the back of the building plate, i.e. K03 and L03, show a shrinkage in comparison with the prototypes at the front of the building plate. Possibly this is due to the gas flow in the printer or due to a position-dependent heat exchange. Based on the measured deviations, the design can be adapted accordingly.

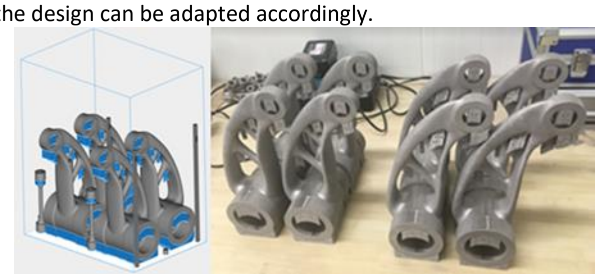

Figure 5. The printing setup of the aerospace components (left) and the printed components (right).

Finally, regarding defect inspection, two main findings are reported from the µ-CT analysis. Firstly, a minimal amount of porosities are detected in the as-printed state for each component. Those pores present a high sphericity and an average equivalent diameter in the range of 330-360 µm, illustrated in Figure 7.

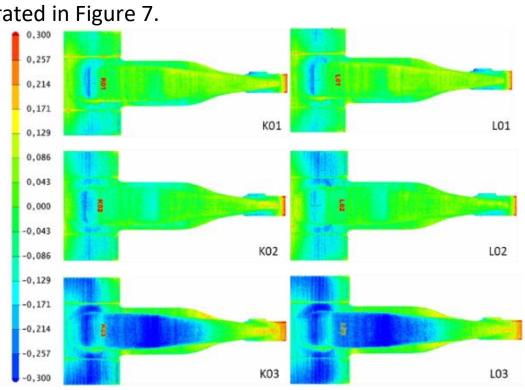

Figure 6. Dimensional quality inspection of the six aerospace components, produced in two batches (max/min: ± 0.3 mm).

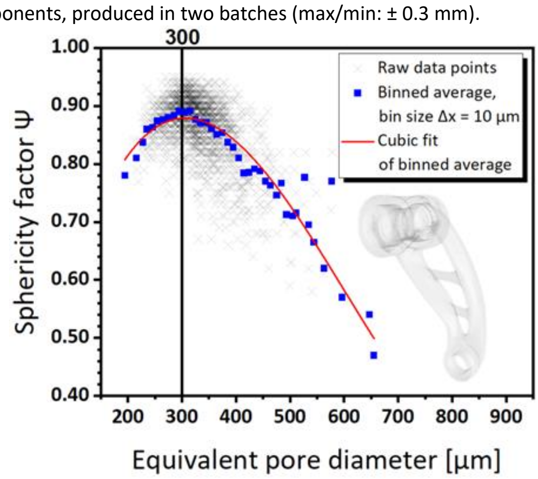

Figure 7. Equivalent pore diameter against the sphericity factor for the sum of porosities identified on the six ALMA prototypes with µ-CT.

The estimated 100 % probability of detection for ⌀ ~> 300 µm is further corroborated by the resulting trend in Figure 7 (red curve), showing how, below 300 µm, sphericity starts to decrease not for a physical process-correlated reason but most probably for the voxelization effect while reaching the resolution limit of the µ-CT analysis. Secondly, some small lack of fusion elongated pores were identified nearby the down-facing surfaces of the parts, down-facing in respect to the direction of fabrication via EBM. This effect can stem from the "thickness function" of the EBM production, which reduces the energy input during the first 2-4 mm of building on top of unmelted powder. The goal of this approach is the avoidance of swelling and bad down-skin surface quality. This second set of porosities might not be completely closed with HIP, if the pores are partially open to the atmosphere due to their proximity to the surface. No cracks were detected, and form deviations confirmed the LLS measurements.

4.3. Post-processing

First, HIP is applied to the components with the intent to close porosities which have a detrimental influence on the mechanical properties, especially fatigue. µ-CT shows that all the as-printed spherical pores are completely closed, or that their size falls below the detectability limit of the µ-CT scan. On the other hand, the lack of fusion elongated pores are not completely eliminated, with few small defects -below 100 µm- still detectable nearby down-facing areas. The measurements with the LLS shows that the volume of the components has decreased. Figure 8 illustrates the comparison of the measurements before and after HIP. The negative deviations indicate a shrinkage of the component. Next, the assembly connections are machined to remove the residuals of the supports and to achieve the profile tolerances of ± 0.6 mm, and the inactive surfaces are dry blasted to guarantee a high surface finishing. The inspection methods are used again to confirm that the end-product meets the specified dimensional tolerances, as depicted in Figure 9.

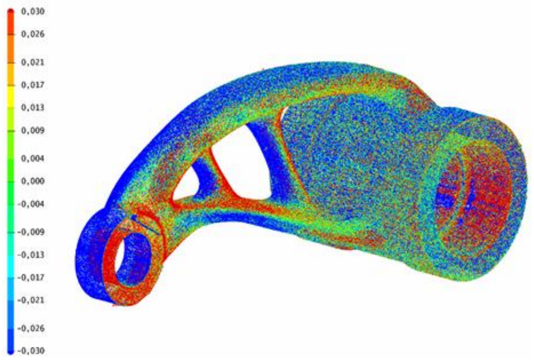

Figure 8. The comparison of the measurements before and after HIP (scale in mm, max/min: ± 0.03 mm).

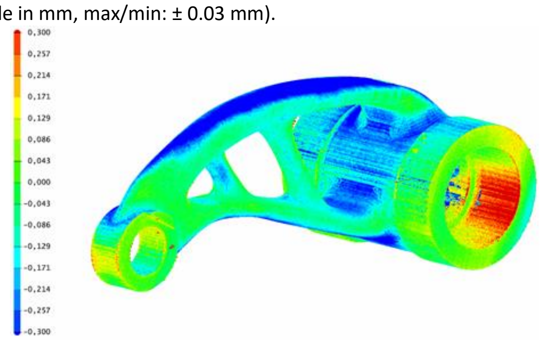

Figure 9. The comparison of the end product and the nominal CAD model (scale in mm, max/min: ± 0.3 mm).

5. Conclusions

This paper discusses all the different steps in the end-to-end production process of an aerospace component. From design of the component via topology optimization and simulation tools, the fabrication through EBM, the post-processing, i.e., HIP and surface finishing, until the measured end-product. The dimensions and inner quality of the produced object are validated with non-destructive tests, i.e. optical scanning and µ-CT, after each stage of the production process. The optical scanning proves that AM is applicable to produce aerospace components when considering dimensional deviations. All prototypes at the end of the production process are within the dimensional tolerances. No porosities or cracks were detected on the final components by µ-CT; however current high energy µ-CT cannot completely reach the QL1-A inspection level required by Airbus specifications for such large parts. For a complete validation and applicability as a structural component, the mechanical properties of the object still need be investigated. The mechanical properties and fatigue tests are investigated within the ALMA project. However, the discussion of these results are not included in this paper.

Acknowledgements

The authors acknowledge the financial support of the Flanders Innovation & Entrepreneurship (VLAIO) through Grant Agreement No. HBC.2018.0427 (SIM-ICON project ALMA). Special thanks to all the partners involved in the project: Bodycote Hot Isostatic Pressing NV: hipping of the prototype; Elsyca NV: surface finishing of the prototype; Materialise NV; Center for Research in Metallurgy (CRM); UGent.

References

[1] Shapiro A A, Borgonia J P, Chen Q N, Dillon R P, McEnerney B, Polit-Casillas R and Soloway L 2016 Additive Manufacturing for Aerospace Flight Applications *J of Spacecraft and Rockets* **53** (**5**) 952–959.
[2] Kerstens F, Cervone A and Gradl P 2021 End to end process evaluation for additively manufactured liquid rocket engine thrust chambers *Acta Astronautica* **182** 454-465.
[3] Anderson D P, Billings K J, Pate A M, Borgonia J P C, Firdosy S A, Voecks G E, Brandon E J and West W C 2022 Topology Optimization and AM for Improving a High-Pressure Electrolyzer Design *J of Materials Engineering and Performance* **31** 6246–6255.
[4] Najmon J C, Raeisi S and Tovar A 2019 Review of additive manufacturing technologies and applications in the Aerospace industry *Additive Manufacturing for the Aerospace Industry* 7-31.
[5] Yusuf S M, Cutler S and Gao N 2019 The Impact of Metal Additive Manufacturing on the Aerospcae Industry *Metals* **209** **9(12)** 1286.
[6] Blakey-Milner B, Gradl P, Snedden G, Brooks M, Pitot J, Lopez E, Leary M, Berto F and du Plessis A 2021 Metal additive manufacturing in Aerospace: A review *Materials & Design* **209** 110008.
[7] VLAIO 2018-2021 ALMA: Additive Layer Manufacturing for Aerospace *SIM-ICON Project* HBC.2018.0427.
[8] Qiu C, Ravi G A, Dance C, Ranson A, Dilworth S and Attallah M M 2015 Fabrication of large Ti–6Al–4V structures by direct laser deposition *J of Alloys and Compounds* **629** 351-361.
[9] Vlaeyen M, Haitjema H and Dewulf W 2021 Digital Twin of an Optical Measurement System *Sensors* **21** 6638.
[10] Wu D, Prado P G, Sinico M and Dewulf W 2022 L0 Regularized Image Deblurring applied to Porosity Analysis in Industrial X-ray Computed Tomography *iCT Conference* **11**.
[11] Sinico M, Bellens S, Van Herreweghen T and Probst G 2021 Exploratory research on the correlation of probability of detection and image quality during the tomographic characterisation of additive manufacturing defects *Adv Prec in Additive Manufacturing*.
[12] Carmignato S, Dewulf W and Leach R 2018 Industrial X-ray Computed Tomography *Springer*.
[13] Booth J W, Alperovich J, Chawla P, Ma J, Reid T N and Ramani K 2017 The design for additive manufacturing worksheet *ASME J of mechanical design*.
[14] Kranz J, Herzog D and Emmelmann C 2015 Design guidelines for laser additive manufacturing of lightweight structures in TiAl6V4 J of Applichations Laser Additive.
[15] Orquéra M, Campocasso S and Millet D 2017 Design for AM method for a mechanical system downsizing *CIRP Design* **27**.
[16] Garibaldi M, Erdelyi H, van Eekelen T and Reznik D 2018 Assessment of a Multi-Scale Approach for Laser Powder Bed Fusion Process Simulation, *NAFEMS Nordic Seminar: Exploring the Design Freedom of Additive Manufacturing through Simulation* Helsinki.